Computation of accelerating electrodes for a relativistic high-current electron beam tube

W. Dommaschk

IPP 0/12 May 1973

MAX-PLANCK-INSTITUT FÜR PLASMAPHYSIK

GARCHING BEI MÜNCHEN

MAX-PLANCK-INSTITUT FÜR PLASMAPHYSIK

GARCHING BEI MÜNCHEN

Computation of accelerating electrodes for a relativistic high-current electron beam tube

W. Dommaschk

IPP 0/12 May 1973

Die nachstehende Arbeit wurde im Rahmen des Vertrages zwischen dem Max-Planck-Institut für Plasmaphysik und der Europäischen Atomgemeinschaft über die Zusammenarbeit auf dem Gebiete der Plasmaphysik durchgeführt.

IPP 0/12 W. Dommaschk

Computation of accelerating electrodes for a relativistic high-current electron beam tube

Abstract

For an axisymmetric high-current electron beam source with plane field emission cathode accelerating field structures around stationary beams of high quality are computed. For this purpose a sufficiently self-consistent mathematical model for the beam is given first. The potential is then continued into the region outside the beam. As in Pierce systems, the surfaces of corresponding accelerating electrodes are determined by equipotential surfaces. The indicated beam model includes self-magnetic fields. It is determined by a system of analytic differential equations which is numerically integrated, except near the cathode, where power series expansions were obtained with the aid of the formula manipulating capability of the computer. The continuation of the potential was made numerically stable by a method due to Garabedian by extending the computation into a fictitious complex domain.

Summary:

1. Introduction

In the development of electron ring accelerators suitable electron sources are required. What is needed is a nearly parallel electron beam a few cm in diameter whose emittance and spherical aberration should be small. The beam energy and current are of the order of a few MeV and several hundred amperes respectively. In our case a source with quasi-stationary electric acceleration and without external magnetic focusing was needed. It had to be operated by a Marx generator. Commercial field emission tubes offered for this purpose fell far short of meeting the beam quality requirements. Investigations were therefore conducted [2, 3, 4] which finally lead to the concept of a new electron source.

This paper concerns the electron optical design of a source with a quasi-plane field emission cathode using pure electric acceleration and beam forming. Among the different approaches for solving this problem as described, for example, in [1], a direct numerical procedure is used which is, in principle, a generalization of the classical Pierce method for axially symmetric beams with a curved boundary. First a solution for the beam region is given which is consistent with Poissons's equation and the equation of motion for the electrons. Furthermore, it can be extended for complex values of the coordinates. This last feature is essential for the potential continuation method described in sec. 3. This solution states Cauchy initial conditions along the curved beam border which have to be satisfied together with the Laplace equation by the potential outside the beam. As is well known, in the real space Cauchy initial conditions where both the value and the normal derivative of the potential are prescribed lead to numerically unstable results since the Laplace equation is elliptic. After a suitable coordinate transformation a numerically stable solution according to Garabedian [8] can, however, be obtained.

The Cauchy conditions and the Laplace equation as written in the transformed coordinates are thereby extended along a fictitious imaginary direction of one coordinate. As is shown in sec. 3, the problem can be restated in this case as an initial-value problem for a hyperbolic partial differential equation which admits numerically stable solutions. This method was successfully applied by Harker [10] in the case of a non-relativistic hollow electron beam. In our case this method yielded reasonable potential distributions in the region of interest around the beam. One of the computed potential configurations was realized by corresponding accelerating electrodes in an actual electron beam source which then proved superior to commercial tubes [5, 6] [1]. Experimental details are given in [6].

2. Solution for the beam

2.1 Beam equations

For the beam region a system of differential equations shall be given which determines the shape of the beam border and the potential distribution in this region. We assume steady-state conditions, rotational symmetry, zero emittance of the beam, no external magnetic field and an equipotential field emission cathode where the initial energy of the electrons is zero. This implies that the particle velocity and the current density in the beam have no azimuthal component. Two further assumptions concern the self-consistency. The beam equations to be given are self-consistent in a practical or numerical sense rather than in a strictly mathematical sense. First it is assumed that

---

[1] Earlier calculations were done in real variables which lead to numerical instabilities. A comparison with the new result from stable calculations (see footnote 3 and Fig.2a) shows agreement with the stable solution up to a few cm from the beam edge.

the beam border is an electron path. Together with the foregoing assumptions this assumption is admissible in any case for a beam of finite length if the slope of all particle paths is sufficiently small. Secondly, the radial variation of the space charge density in the beam is assumed to be a linear function of the radial potential difference whose coefficients depend on the axial position. As can be seen below, this assumption is admissible in any case if the slope of the particle paths, the relative radial potential difference in the beam and the relative radial current density variation are sufficiently small relative to unity. This also implies sufficiently homogeneous emission at the cathode. These self-consistency assumptions are largely justified by the results. The maximum slope of the beam border is in most cases less than 100 mrad. The maximum relative radial variation of the space charge density with the potential amounts to a few per cent only. The maximum angular deviation in the slope of the beam border from the virtual focus point of a paraxial electron path was found to be less than 5 mrad in all cases. This should also indicate a small current density variation over the beam cross section. Even if this were not the case, this would have little influence on the potential and the normal electric field at the beam border which finally determine the potential distribution outside the beam. This is so because these quantities are mainly determined by the given constant value of the total beam current rather than by the special shape of the internal current density distribution.

The paths of the electrons are determined by the equation of motion:

$$d(m_o \gamma \vec{v})/dt = -e(\vec{E} + \vec{v} \times \vec{B}) \qquad (1)$$

where t is the time, γ the relativistic mass ratio, $\vec{v}$ the velocity vector, $e > 0$ the electron charge, m_o the rest mass, $\vec{E}$ the electric field vector and $\vec{B}$ the vector of the magnetic induction. From the steady-state assumption we have:

$$\vec{E} = -\nabla U \tag{2}$$

where U is the potential. Since $\nabla\vec{E} = \sigma/\varepsilon_o$, where σ is the space charge density and ε_o the vacuum dielectric constant, U obeys Poissons's equation:

$$\Delta U = -\sigma/\varepsilon_o \tag{3}$$

where the space charge density is related to the current density vector $\vec{j}$ by:

$$\vec{j} = \sigma\vec{v} \tag{4}$$

We introduce the axial and radial coordinates z and ϱ respectively, where z = 0 at the cathode. The potential is normalized according to $\varphi = U/U_o$, where $U_o = m_o c^2/e$ and c is the velocity of light. If $\varrho = R(z)$ describes the shape of the beam border, we use the following representation for the normalized potential φ, which shall be valid in the range $0 \le \varrho \le R(z)$:

$$\varphi(z,\varrho) = \phi(z) + \vartheta(z,\varrho), \text{ where:} \tag{5}$$

$$\vartheta(z,\varrho) = \sum_{n=1}^{N} \psi_n(z)(B_n(\varrho) - B_n(0)) \tag{5a}$$

Here the integer N is to be given. The problem is to determine the unknown functions R(z), $\phi(z)$, $\psi_n(z)$, $B_n(\varrho)$ for n=1,2,..,N. If these are given, the Cauchy conditions for the subsequent potential continuation can be determined from them (see sec. 3). In eqs. (5), (5a) ϕ is the normalized potential at the beam axis ($\varrho = 0$) and ϑ, which is zero at the axis, is the normalized radial potential difference. From the normalized potential the relativistic mass ratio γ and velocity ratio β are given by:

$$\gamma(\varphi) = 1 + \varphi \quad \text{and} \tag{6}$$
$$\beta(\varphi) = (\varphi(2+\varphi))^{1/2}/(1+\varphi)$$

Because of the foregoing assumptions the magnetic induction has only an azimuthal component B. If $I > 0$ denotes the total electron beam current, which is a constant, it follows from the Stokes theorem:

$$B(\varsigma) = -I\mu_o/2\pi\varsigma \qquad \text{for } \varsigma \geq R(z) \tag{7}$$

where μ_o is the vacuum permeability. In accordance with the first self-consistency assumption the radial component of eq. (1) yields a differential equation for R(z) if z is introduced instead of t in this equation. We use the normalized beam current $K = I/\pi U_o c \varepsilon_o$, where $c = (\varepsilon_o \mu_o)^{-1/2}$, and get:

$$d(\beta\gamma R'/\sqrt{1+R'^2})/dz = (\partial\varphi/\partial\varsigma)\cdot\sqrt{1+R'^2}/\beta - K/2R \tag{8}$$

where $R' = dR/dz$ and γ, β and $\partial\varphi/\partial z$ are to be evaluated at $\varsigma = R(z)$ from the above expressions. The equations which determine the unknown functions in eqs. (5), (5a) have to be obtained from Poissons's equation. For this purpose a suitable expression for the space charge density must first be given. From eq. (4) we get $\sigma = |\vec{j}|/|\vec{v}|$ and $j_z/|\vec{j}| = v_z/|\vec{v}|$, where j_z and v_z are the axial components of $\vec{j}$ and $\vec{v}$ respectively. If $\varsigma = r(z)$ is an electron path somewhere in the beam and $r' = dr/dz$, we have $|\vec{v}|/v_z = (1+r'^2)^{1/2}$ and get:

$$\sigma = j_z(1+r'^2)^{1/2}/\beta c \tag{9}$$

If $\vartheta \ll \varphi$ or $1-\beta \ll 1$ a first-order Taylor expansion of $1/\beta$ with respect to ϑ can be made in this expression. In accordance with the assumptions, r' and the relative change of $j_z = j_z(z,\varsigma)$ with respect to ς should be small relative to unity. In this case the numerator of eq. (9) can be replaced by its approximate average $\langle j_z(1+r'^2)^{1/2}\rangle \approx \langle j_z\rangle\cdot(1+\langle r'^2\rangle/2)$ over the beam cross section. The average of j_z is obviously given by $\langle j_z\rangle = -I/\pi R^2(z)$. Since under our conditions all electron paths are nearly similar to each other, we assume $r' \approx rR'/R$ to get the average of r'^2, which is $\langle r'^2\rangle \approx R'^2/2$ in this case. The

resulting expression for σ can now be inserted into eq. (3), which yields for the normalized potential φ :

$$\Delta\varphi(z,\varsigma) = F_o(z) - F_1(z)\vartheta(z,\varsigma) \text{ where} \tag{10}$$

$$F_o(z) = K(1+R'^2(z)/4)/R^2(z)\beta(\phi(z)) \tag{10a}$$

$$F_1(z) = K/R^2(z)\beta^3(\phi(z))\gamma^3(\phi(z)) \tag{10b}$$

After inserting the explicit expressions eq.(5) and eq.(5a) for φ and ϑ into eq.(10), this equation must be satisfied for independent and arbitrary values of z and ς . This is the case if the functions in the expression for φ are determined by:

$$\phi'' = F_o(z) - \sum_1^N \psi_n \tag{11}$$

$$\psi'' = -(F_1(z)+\lambda_n^2)\psi_n, \text{ for } n = 1,2,\ldots,N \tag{12}$$

$$B_n(\varsigma) = J_o(i\lambda_n\varsigma)/\lambda_n^2, \text{ for } n = 1,2,\ldots,N \text{ where} \tag{13}$$

$$B_n(\varsigma) - B_n(0) = (\varsigma/2)^2\sum_{k=o}^{\infty}(\varsigma\lambda_n/2)^{2k}/((k+1)!)^2 \tag{14}$$

$$B_n'(\varsigma) = (\varsigma/2)\cdot\sum_{k=o}^{\infty}(\varsigma\lambda_n/2)^{2k}/(k!(1+k)!) \tag{15}$$

Here primes denote differentiation with respect to z or ς; λ_n^2 for n = 1,2,..., N are separation constants; $i = \sqrt{-1}$ and J_o is the zero-order Bessel function. Together with eq.(8) and related equations these equations determine a solution for the beam region. Simultaneous integration yields the potential inside the beam together with the form of the beam border R(z). Since analytic integration is hopeless except near the cathode (see below), it must be done numerically. By selecting a proper set of "eigenvalues" λ_n^2 the corresponding "eigenfunctions" $\psi_n(z)$ and the radius dependent part of the potential can be made to meet certain boundary conditions and focusing properties. The number of eigenfunctions to be used is arbitrary, though a

reasonable continuation of the potential seems more likely to be obtained with a small number. In the examples (see Appendix) tube configurations with a first grid in front of the cathode and sometimes a second grid in the anode aperture were investigated. In these cases all ψ_n in eqs.(5a,11,12) were put to zero between the cathode and the first grid and only ψ_1 was maintained between the first grid and the anode.

Solutions not using the first grid can also be obtained, at least in principle. In this case more than one eigenfunction must be used to achieve approximately a radially constant electric field at the cathode. The case that all eigenfunctions are deleted or zero seems impracticable without a first grid and with the usual currents because of the magnetic contraction. As follows from eqs.(5), (5a), the conditions $\vartheta = 0$, $\partial\vartheta/\partial\varrho\partial z = 0$ must be satisfied at the cathode (z=0) to achieve a constant field there. If $N > 1$ is the number of eigenfunctions these conditions are satisfied up to and including the power ϱ^{2N-2} in eqs.(5a) and (14), provided that the initial values of the eigenfunctions are given or related by:

$$\psi_n(0) = 0, \qquad n = 1,2,3,\ldots,N \tag{16}$$

$$\sum_{n=1}^{N} \psi_n'(0)\lambda_n^{2m} = 0, \qquad m = 0,1,2,\ldots,N-2 \tag{17}$$

and if the contribution from higher powers of ϱ to $\partial\varphi/\partial z$ at $z = o$ can be neglected. From eqs.(12) the power series expansion of ψ_m near $z = 0$ can be seen to have the form $c_1 z + c_2 z^{3/2} + \ldots$, where c_1, c_2 are constants. Thus $\psi_n'(0)$ is finite and eqs.(16), (17) can be satisfied. In any case the node distance of the lowest order eigenfunction must not fall short of the tube length L. Thus $\lambda_1 < \pi/L$ is obtained from eqs.(12). This indicates a fast convergence of the series eq.(14) for low order eigenvalues if the cathode radius is small relative to L. A small number of eigenfunctions might therefore be sufficient to yield constant field conditions at the cathode by eqs.(16),(17). Of course, a careful examination of all possible errors would be necessary.

2.2 Power series solution near the cathode:

At the cathode the differential equations (8), (11) and (12), which determine the solution inside the beam, all become singular because β approaches zero. It is therefore necessary to do the first integration step by using a power series expansion before the numerical integration can be started. A corresponding solution which holds near z = 0 was obtained by means of the REDUCE 2 formula manipulating capability of the computer. In the actual calculations the length of the first step was chosen to be small relative to the beam radius. But the series could just as well be used to estimate the beam parameters up to the first grid in most cases. According to the assumed conditions in this part the potential is radially constant. Since R'^2 is small and practically zero during the first step, this quantity is neglected relative to unity in this case. Therefore, the power series solution has to be found from the equations:

$$d(\beta\gamma\eta')/dz = -\bar{K}/2\,\eta \tag{18}$$

$$\phi'' = \bar{K}/\beta\gamma^2 \tag{19}$$

where $\bar{K} = K/R^2(0)$, R(0) is the beam radius at the cathode (z=0) and $\eta = R(z)/R(0)$ is the relative beam radius. The constant K is given in conjunction with eq.(8). With the proper initial conditions $\phi(0)=0$, $\phi'(0)>0$, $\eta(0)=1$, $\eta'(0)=0$ it can be seen from eqs.(18), (19) that the series for both ϕ and η begin to proceed with half integer powers of z. Thereby the lowest power in ϕ is z, and the lowest power in η -1 is $z^{3/2}$. We introduce $\mu = \bar{K}^{1/4}z^{1/2}$, $p = (2\phi'(0))^{1/2}/\bar{K}^{1/4}$ and write:

$$\phi = p^2\mu^2/2 + P_3\mu^3 + P_4\mu^4 + \ldots \tag{20}$$

$$\eta = 1 + Q_3\mu^3 + Q_4\mu^4 + \ldots \tag{21}$$

By using μ instead of z as independent variable in eqs.(18), (19) these equations become formally independent of $\overline{K}$. We further insert γ, β from eq.(6) with $\varphi = \phi$ and eqs.(20),(21) into these equations and carry out the differentiations with respect to μ. By rearranging the resulting equations all denominators and square roots can be removed. By equating equal powers of μ the coefficients P_k, Q_k can be successively computed to give:

$$
\begin{aligned}
P_3 &= 4/3p \\
P_4 &= -2/3p^4 \\
P_5 &= (9p^8 + 80)/90p^7 \\
P_6 &= 8(9p^8 - 80)/405p^{10} \\
P_7 &= -(135p^{16} + 6624p^8 - 98560)/30240p^{13} \\
&\cdots\cdots\cdots\cdots
\end{aligned}
\qquad (22)
$$

$$
\begin{aligned}
Q_3 &= -1/3p \\
Q_4 &= 1/3p^4 \\
Q_5 &= (3p^8 - 80)/120p^7 \\
Q_6 &= (9p^8 + 640)/405p^{10} \\
Q_7 &= -(405p^{16} + 2208p^8 + 492800)/120960p^{13} \\
&\cdots\cdots\cdots\cdots
\end{aligned}
\qquad (23)
$$

A practical evaluation shows that the series are semi-convergent. They will diverge for larger values of z or μ because of the nearby singularities at $\eta = 0$ and $\phi = -2$. For our purpose their minimum term is however small enough.

If power series solutions for cases without a first grid are desired, the full set of equations (8), (11) and (12) must be solved with the only simplification that η'^2 can be neglected relative to unity. As compared with the above series, the larger number of parameters would then lead to much more complicated expressions.

2.3 Spherical aberration

The spherical aberration corresponds to an error δ_α in the slope of the beam boundary:

$$\delta_\alpha = R' - R'_p R/R_p \tag{24}$$

where R_p is the radius of a "paraxial" electron beam. Since R' is small, δ_α is the angular deviation of a tangent to the beam boundary from the axial intersection point of a tangent to the paraxial beam at the same axial position. The paraxial beam equation follows from eq.(8) in the case that the beam radius and the slope of the beam boundary go to zero. The constant K is thereby changed to $K_p = KR_p^2(0)/R(0)$ since K contains the total beam current. The paraxial radial electric field follows from eq.(10), which is written as $\Delta\varphi = K_p/\beta(\phi)R_p^2$ in the paraxial region. Its paraxial solution is $\varphi = \phi + (\varrho^2/4)\times (K_p/\beta(\phi)R_p^2 - \phi")$. At the paraxial beam boundary we therefore have:

$$(\partial\varphi/\partial\varrho)_{\varrho=R_p} = K_p/2\beta(\phi)R_p - \phi"R_p/2 \tag{25}$$

This leads to the well known paraxial beam equation:

$$d(\beta(\phi)\gamma(\phi)R'_p)/dz = (K_p/\beta(\phi)\gamma^2(\phi)R_p - \phi"R_p)/2\beta(\phi) \tag{26}$$

It is given in, for example, [9], where an external magnetic field is also included. This equation can be simultaneously integrated together with eqs.(8), (11) and (12) to get R_p and δ_α from eq.(24). Since $K_p \sim R_p^2(0)$ and $R'_p(0) = 0$, eq.(26) shows that $R_p \sim R_p(0)$ and δ_α is therefore independent of $R_p(0)$. For this reason we can use:

$$R_p(0) = R(0) \quad \text{and} \quad K_p = K \tag{27}$$

In the cases computed up to now the error δ_α was found to be of the order 10^{-3} or less. The corresponding relative difference

$R/R(0) - R_p/R_p(0)$ between the paraxial and the nonparaxial beams amounted to a few per cent.

For the first part of the beam δ_α can also be estimated analytically. This is again done with the aid of REDUCE 2 by a power series expansion of eqs.(18), (19), where the additional factor $(1 + \eta'^2 R^2(0))^{-1/2}$ is inserted into the parentheses on the left side of eq.(18). It is thereby assumed that ϕ is unchanged. Inserting $\eta R(0)$ from the old and new expansions as R_p and R respectively into eq.(24) yields:

$$\delta_\alpha = (\mu^3 K^{3/2}/\eta p^3)(0.073376 - 0.021751\mu/p^3 \pm \ldots) \qquad (28)$$

Here K is given in conjunction with eq.(8), μ, p and η are given in sec. 2.2. Higher terms show that the series is again semi-convergent. For the present purpose the first two terms given in eq.(28) are sufficient.

2.4 Space charge error and improved beam equations

We assume a constant current density distribution at the cathode and approximate the residual radius dependence of the axial current density caused by the spherical aberration by $j_z = A + B\varsigma^2$, where A and B depend on z and $B\varsigma^2$ is small relative to A. Making use of eq.(27) we have $A = -I/\tilde{\pi}\varsigma_p^2$ and B is determined from the condition that the integral of $-j_z$ over the beam cross section $R^2\tilde{\pi}$ is equal to the total beam current I. This yields:

$$j_z = -(I/R^2\tilde{\pi})(R^2/R_p^2 + 2(1 - R^2/R_p^2)\varsigma^2/R^2) \qquad (29)$$

Using eqs.(9) and (29) the maximum relative error δ_s on the right side of eq.(10) due to the spherical aberration can be estimated to be:

$$|\delta_s| \approx |R^2/R_p^2 - 1 - R'^2/4| \qquad (30)$$

Its observed order of magnitude was 10^{-2} or less. Another error δ_β is caused by neglecting higher Taylor expansion terms of $1/\beta$ in eq.(9), being given by:

$$|\delta_\beta| \approx 3\vartheta^2/2\beta^4(\phi)\gamma^4(\phi) \qquad (31)$$

where ϑ corresponds to the potential difference between the beam axis and the beam border in this case. This error can be kept small if ϑ is zero or goes to zero faster than z near the cathode. The same condition is necessary to get a constant field and a homogeneous current density distribution at the cathode plane. In the examples given in sec. 7[5] this was realized by dividing the beam into two parts by a plane grid electrode where $\vartheta = 0$ in the first part. In these cases δ_β is of the order of 10^{-3} or less. In the examples given the space charge error is thus mainly determined by δ_s.

The potential and electric field errors which are effectively caused by the space charge error correspond to a solution of the Poisson equation for this error in the actually calculated and realized electrode system under the condition that the erroneous potential is zero at all electrodes. If the relative error were constant and equal to δ in the beam region, the potential error would be about δ times the source part of the calculated potential distribution. Its absolute maximum would occur at the beam axis and away from the electrodes. The corresponding electric field error would have its maximum at electrode surfaces near the beam.

At the cathode the source part of the electric field due to space charges can be found to reach up to about 250 kV/cm. For $\delta \approx \delta_s \approx 10^{-2}$ this would correspond to local field errors of up to 2.5 kV/cm and corresponding potential errors of up to about 1 kV because the distance of the first grid from the cathode is of the order of 1 cm. For this reason compensating relative deviations up to δ_s from a homogeneous emission can be expected at the cathode because the field emission depends very strongly

on the electric field. The actually remaining axial field error should then be small relative to 2.5 kV/cm. This applies all the more so to the corresponding erroneous radial electric fields between the cathode and the first grid since the mean space charge error in the beam cross section was practically set equal to zero by averaging (eqs.(9) to (10)). In addition, radial fields are largely shorted owing to the nearby electrodes. The erroneous radial electric field should be uncritical if the corresponding force is small relative to the magnetic forces at the beam border. The normalized mean radial electric field E_f which would be equivalent to the magnetic focusing effect at the beam border up to the first grid can be estimated by equating corresponding integrals over the magnetic and electric terms on the right side of eq.(8):

$$\int_0^{z_s} dz E_f/(2z\phi'(0))^{1/2} \gtrsim \int_0^{z_s} dz E_f(1+R'^2)^{1/2}/\beta = \int_0^{z_s} dz K/2R \geq z_s K/2R(0)$$

or:
$$E_f \gtrsim K(z_s\phi'(0)/8)^{1/2}/R(0) \qquad (32)$$

where z_s is the distance of the first grid from the cathode. For a cathode radius of 1 cm, z_s = 1 cm and a total emission of 1000 A we have K = 0.235, $\phi'(0) \approx 0.5$ and get $E_f \gtrsim 0.06$, which corresponds to 511 x 0.06 $\approx$ 30 kV/cm. This is much larger than the possible field error. For this reason the focusing properties of the section between the first two electrodes should be very insensitive with respect to errors in the self-consistency assumptions. For the same reason small irregularities such as might be introduced by the finite beam emittance or by inhomogeneous emission should be uncritical.

In the second part of the beam between the first grid and the anode the above-mentioned relative current density variation up to δ_s appear which were generated by inhomogeneous emission. In addition, the relative space charge error δ_s is present. Both effects may cumulate to $\delta \approx 2\,\delta_s$ but in any case their radial average is practically zero because the total beam current is assumed to be constant. If the average of δ is not

zero, its effect may be estimated by using the model of a cylindrical relativistic electron beam. In this case the electrical field at the beam edge is $60I/R\beta$ in V/cm and the radial potential difference in the beam is about $30I/\beta$ in V. This corresponds to about 60 kV/cm and 30 kV respectively for a relativistic 1 kA beam of 1 cm radius. A space charge error of 1 per cent corresponds to 600 V/cm and 300 V respectively. The beam border deviation $\Delta R'$ caused by this radial electric field can be estimated from eq.(8) by $d(\beta\gamma\Delta R')/dz \approx 600/5.11 \times 10^5\beta$. This yields $\Delta R' \approx 6$ mrad over a beam length of 20 cm if β on the right side is assumed to be constant corresponding to 1 MeV and the end energy of the beam is 2 MeV If a linear growth of $\Delta R'$ is assumed, this corresponds to a radial displacement $\Delta R \approx 0.6$ mm over the same length. If the space charge error were caused by an error in the current density, then $\Delta R'$ and ΔR would be reduced by the average of $1/\gamma^2$. Thus space charge errors should not be critical, especially if they result from an erroneous current density. For this reason drastic changes due to the finite emittance of the actual beam are not to be expected as was also the case in the first part of the beam.

With increased computational effort more exact beam equations are possible where radial averaging in the space charge density is not necessary. Substituting eq.(29) into eq.(9) and using $(1 + r'^2)^{1/2} \approx 1 + r'^2/2$, where $r' \approx \varsigma R'/R$, we obtain instead of eq.(10):

$$\Delta\varphi = F_o^* - F_1^*\vartheta(z,\varsigma) + F_2^*\varsigma^2 \qquad (10^*)$$

$$F_o^* = K/R_p^2\beta(\phi) \qquad (33)$$

$$F_1^* = K/R_p^2\beta^3(\phi)\gamma^3(\phi) \qquad (34)$$

$$F_2^* = 2K(R_p^2/R^2 - 1 + R'^2/4)/R^2R_p^2\beta(\phi) \qquad (35)$$

Instead of eq.(5a) we use:

$$\vartheta(z,\varrho) = \sum_n \Psi_n(z)(B_n(\varrho) - B_n(0)) + \varrho^2 g(z) \qquad (5a^*)$$

The function $g(z)$ is used to remove terms which depend explicitly on ϱ^2 from eq.(10*). For this reason $g(z)$ is to be determined by:

$$g'' = F_2^* - gF_1^* \qquad (36)$$

Instead of eqs.(10a) and (10b) we use:

$$F_o = F_o^* - 4g \qquad (10a^*)$$

$$F_1 = F_1^* \qquad (10b^*)$$

This again leads to eqs.(11) to (15). The new set of beam equations is now given by eqs.(8), (11), (12), (13) and (36). Numerical evaluation of this set has not yet been made. The results shown in the appendix were obtained with the aid of the original beam equations (sec. 2.1).

3. Continuation of the potential

The mathematical procedure to determine the potential outside the beam region is similar to that used by Harker [10]. First the original initial-value problem for the Laplace equation is formulated in suitable coordinates. For this purpose the following coordinate transformation is made which maps the real z-ϱ plane into the real u-v plane and the beam border $\varrho = R(z)$ into the u-axis at v=0:

$$z + i\varrho = iR(u + iv) + u + iv \quad \text{or:} \qquad (37)$$

$$z = (i/2)(R(u + iv) - R(u - iv)) + u \qquad (37a)$$

$$\varrho = (1/2)(R(u + iv) + R(u - iv)) + v \qquad (37b)$$

Since this transformation is conformal, the new u-v coordinates are orthogonal to each other and the Laplace equation is of the form [11] :

$$\partial(\varsigma\partial\varphi/\partial u)/\partial u + \partial(\varsigma\partial\varphi/\partial v)/\partial v = 0 \qquad (38)$$

Here ς is to be expressed by eq.(37b) as a function of u and v. This equation has to be solved in a limited region for $v \geq 0$ and φ must satisfy the following Cauchy initial conditions along the u-axis at v=0:

$$\varphi = \varphi(z,\varsigma),\ \partial\varphi/\partial v = \varphi_\varsigma - \varphi_z R'(z),\ \text{for } z = u,\ \varsigma = R(u) \qquad (39)$$

Here $R' = dR/dz$ and φ_ς, φ_z are the expressions for the partial derivatives of φ with respect to ς and z obtained from eqs.(5), (5a) and (13). Since eq.(38) is elliptic, an attempt to solve this problem by finite difference methods in the real u-v plane leads to numerically unstable results even if the true solution is regular. As shall now be shown, this problem can, however, be reformulated in the form of a well posed hyperbolic initial-value problem if an analytic continuation of the Cauchy initial conditions eq.(39) for complex values of u is available. In this case numerically stable results can be obtained for regions where the true solution has no singularities.

We extend u to complex values and write:

$$u = x + iy \qquad (40)$$

where x, y and v remain real. Correspondingly, φ is extended for complex values of u (where φ becomes complex). Since for analytic functions $\partial/\partial u = \partial/\partial(iy)$, the Laplace equation (38) may be rewritten as:

$$\partial(\varsigma\partial\varphi/\partial y)/\partial y - \partial(\varsigma\partial\varphi/\partial v)/\partial v = 0 \qquad (41)$$

where ζ is complex since it is to be expressed by eq.(37b) for complex values of u. Eq.(41) is hyperbolic and has the real characteristics v = const ± y. The derivatives in this equation with respect to y and v mean that the other two coordinates x, v and x, y respectively are kept constant. If φ is looked at as a function in the x-y-v space, it obeys an elliptic equation in the original plane y = 0 (which is the real u-v or z-ζ plane) but obeys a hyperbolic equation within planes x = const which are orthogonal to the original plane. The beam equations in sec. 2 can also be extended for complex values of u. For this reason they are written as a set of simultaneous first-order differential equations:

$$d\mathfrak{W}/dz = \mathfrak{U}(\mathfrak{W}) \qquad (42)$$

where the components of $\mathfrak{W} = \mathfrak{W}(z)$ are given by $R'(z)$, $R(z)$, $\phi'(z)$ $\phi(z)$, $\Psi_1'(z)$, $\Psi_1(z)$, ..., $\Psi_N(z)$. The components of $\mathfrak{U}(\mathfrak{W})$ are the right sides of the corresponding componential differential equations which may easily be obtained from eqs.(8), (11) and (12). First eq.(42) is integrated for real values of the argument z. Then an extension of $\mathfrak{W}(z)$ for $y \neq 0$ is made within the plane v = 0 as follows. Under the conditions x = const and v = const = 0 we obtain from eqs.(37a) and (40) $d\mathfrak{W}/dy = (d\mathfrak{W}/dz)(dz/dy) = id\mathfrak{W}/dz$ or with eq.(42):

$$d\mathfrak{W}/dy = i\mathfrak{U}(\mathfrak{W}), \text{ for } x = \text{const and } v = \text{const} = 0 \qquad (43)$$

Starting at x = 0 and v = 0, where z = x is real and the initial value $\mathfrak{W}(x)$ is known from the previous integration, eq.(43) can also be integrated. This yields a complex $\mathfrak{W}(z)$ for the complex argument $z = u = x + iy$ at v = 0, where $\zeta = R(u)$ and R(u) becomes complex, too.

With these results φ, φ_ζ, φ_z and $\varphi_v = \partial\varphi/\partial v$, i.e. the Cauchy initial conditions eq.(39) can also be extended for complex

values of u. From eqs.(5), (5a), (13) and (39) we obtain for $v = 0$, $u = x + iy$:

$$\varphi = \phi(u) + \sum_1^N \psi_n(u)(J_o(i\lambda_n R(u))-1)/\lambda_n^2 \tag{44}$$

$$\varphi_z = \phi'(u) + \sum_1^N \psi_n'(u)(J_o(i\lambda_n R(u))-1)/\lambda_n^2 \tag{45}$$

$$\varphi_\zeta = -\sum_1^N i\psi_n(u)J_1(i\lambda_n R(u))/\lambda_n \tag{46}$$

$$\varphi_v = -\sum_1^N \left[i\psi_n(u)J_1(i\lambda_n R(u))/\lambda_n + R'(u)\psi_n'(u)\cdot (J_o(i\lambda_n R(u))-1)/\lambda_n^2\right] - \phi'(u)R'(u) \tag{47}$$

where J_1 is the first order Bessel function.

The solution of the whole continuation problem can now be illustrated with the aid of fig.1a and 1b. fig.1a shows the real $z - \zeta$ plane which corresponds to the plane $y = 0$ in fig. 1b. The portion AB of the curved beam border maps into the straight line A'B' at the x-axis in fig.1b. The triangle E'D'C' in fig.1b is parallel to the y-v plane, i.e. normal to the x-axis. It is bounded by the straight lines $v = 0$, $v = L - y$ and $v = L + y$ for $x = \text{const}$, where the last two lines are characteristics of eq.(41). The straight line B'C' in this triangle maps into the curved part BC in fig.1a, which intersects the beam border at B at right angles. Eq.(42) is now integrated from A to B or A' to B'. Eq.(43) is then integrated from B' to D' and complex Cauchy initial conditions are generated there by eqs.(44) to (47). With these initial data the hyperbolic equation eq.(41) can be solved in the triangle B'D'C' by a stable finite difference algorithm. At $y = 0$, where φ must be real, the reflection principle is used as a boundary condition along B'C'. This principle states in our case that any regular complex function which is real at $y = 0$ changes to its complex conjugate if the sign of y is reversed. After the solution of eq.(41) φ is known at discrete points along B'C'. The $z - \zeta$ coordinates of these points are obtained by eqs.(37a)

and (37b). The potential is thus finally found at discrete points along the curve BC (which is not an equipotential line!) in the original real z - ζ plane in fig.1a. The potential distribution outside the beam is thus obtained by repeating the described process for a sufficiently large number of points B along the beam border.

4. Numerical solution

The numerical integration of eqs.(42) and (43) was done by the usual library subroutines. The right sides of eq.(43) were thereby computed in complex arithmetic and numerically split into their real and imaginary parts to get the two corresponding real differential equations. For the hyperbolic partial differential equation (41) the following simple explicit difference algorithm was used:[2)]

$$\varphi_4 = \frac{\varphi_1(1-h\zeta_y/2\zeta) - \varphi_2(1-h\zeta_v/2\zeta) + \varphi_3(1+h\zeta_y/2\zeta)}{1+h\zeta_v/2\zeta} \qquad (48)$$

The complex potentials φ_1 to φ_4 are thereby taken at the relative positions 1, 2, 3, 4 around some intermediate point o, as indicated in fig.2, h is the mesh size which was made equal in both directions and ζ together with its partial derivatives ζ_y, ζ_v is to be taken at the intermediate point o. Fig.2 corresponds to the triangular area B'D'C' in fig.1b. The origin k = j = 0 in fig.2 thereby corresponds to point B' and the dotted line indicates the charateristic v = L - y of fig.1b. From the previous integration of eq.(43) $R' = R'_m$, $R = R_m$, ..., $\Psi'_N = \Psi'_{N',m}$, $\Psi_N = \Psi_{N',m}$ are given at equidistant discrete points y = hm for m = k = 0, 1, 2, ... at j = 0 in fig.2. At the mesh point o, whose position is described by the integers j and k, we then get from eqs.(37b) and (40):

---

2) Eq.(48) is not yet well adapted to the nearby logarithmic singularity of φ at the beam axis. This may lead to slight systematic numerical deviations from $\Delta\varphi = 0$ at increasing distances from the beam axis especially at small beam radii and large beam currents. In addition, the step length ratio h_v/h_y which is equal to unity in this equation may possibly be decreased to improve the numerical stability.

$$\zeta = (1/2)(R_{k+j} + R_{k-j}) + hj \tag{49}$$

$$\zeta_v = (i/2)(R'_{k+j} - R'_{k-j}) + 1 \tag{50}$$

$$\zeta_y = (i/2)(R'_{k+j} + R'_{k-j}) \qquad \text{and} \tag{51}$$

$$R_{-m} = R^*_m, \; R'_{-m} = R'^*_m \tag{52}$$

where the asterisk denotes the complex conjugate.

Thus ζ, ζ_v and ζ_y are known functions of the position of the intermediate mesh point o. Eq.(48) is evaluated at the consecutive positions $j = 0$, $k = 1, 3, 5, \ldots, k_L - 1$, $j = 1$, $k = 0, 2, 4, \ldots, k_L - 2$, $j = 2$, $k = 1, 3, 5, \ldots, k_L - 3$, ... of the intermediate point o. If $k = 0$, φ_1 is given as the complex conjugate of φ_3. If $j = 0$, φ_1 and φ_3 are given by eq.(44) for $m = k - 1$ and $m = k + 1$ respectively. In this case φ_2 is given by:

$$\varphi_2 = (\varphi_1 + \varphi_3)/2 - \varphi_v h - (1 + R'^2_k)\varphi_\zeta h^2/2R_k \tag{53}$$

where φ_ζ and φ_v are given by eqs.(46) and (47) for $m = k$.

At the end of this calculation real values of φ result at the points $k = 0$, $j = 0, 2, 4, \ldots$ in fig.2, whose z and ζ-coordinates are given according to eqs.(37a) and (37b) by:

$$z = (i/2)(R_j - R^*_j) + x \tag{54}$$

$$\zeta = (1/2)(R_j + R^*_j) + hj \tag{55}$$

Points in the z-ζ plane corresponding to prescribed potential values can be found by interpolation. After repeating the whole continuation process for a sufficiently large number of different x-values and after topological ordering of the interpolated points, equipotential lines can be drawn by the usual plotting routines.

5. Results

Results of the computation are presented in fig.2a to fig.5 in the appendix. In all figures the beam propagates from left to right. The straight horizontal dotted line corresponds to the axis of symmetry, the curved nearly horizontal line is the beam border, the straight vertical part of the leftmost line corresponds to the emitting area of the cathode and the two vertical dotted lines indicate the first and second grids (if present). All other lines correspond to equipotential surfaces obtained by the described continuation process. Owing to the different form of the beam equations used at either side of the first grid, two different equipotential surfaces of equal potential emerge from the grid. They do not overlap and can thus be realized by the surfaces of a solid electrode as indicated.

Fig.2a shows a comparison between the described continuation method with an earlier result [4, 6] which was originally obtained by an unstable calculation in the real domain.[3] The short equipotential lines correspond to the earlier calculation, whereas the radially more extended lines were obtained by the described method. As can be seen, there is good agreement in the shape of the lines near the beam border. The earlier calculation stopped, however, after a few cm because of instabilities. No such instabilities were, however, encountered with the new method, which indicates their purely numerical nature.

In fig.3 the potential lines emerging from a saddle point were nearly obtained (1.86 MV lines). The figure indicates that the lines at an off-axis saddle point intersect at right angles as is to be expected. This figure is also an example of a tube without a second grid. The left part of the 1.86 MV line or some adjacent line can be replaced by an actual electrode without a grid. This is again shown in the following figures where the corresponding equipotential lines have a potential of 2 MV as is desired in our case.

---

[3] In this earlier calculation the equipotential lines were directly calculated in the real ϱ-z plane in the form $z = z(\varrho,\varphi)$ by the equation $\partial^2 z/\partial\varrho^2 = -(\partial z/\partial\varrho)/\varrho + \partial((1 + (\partial z/\partial\varphi)^2/(\partial z/\partial\varphi))/\partial\varphi$, which corresponds to the Laplace equation.

Fig.4 corresponds to an electron source without a second grid which yields a weakly divergent electron beam about 2 cm in diameter, 1 kA and 2 MeV. The grid electrode at 322 kV with respect to the cathode is placed 1 cm distant from the emission area (3 cm in diameter), at whose surface a field strength of 230 kV/cm is maintained at a total emission of 1.2 kA. Field strengths of this order of magnitude are necessary, for example, at quasi-plane cathodes made from stacked razor blades [6]. Between the cathode and the grid all ψ_n in the beam equations (6), (7) were set equal to zero, corresponding to $\vartheta = 0$, to get the conditions for homogeneous emission. This is also the case in all other examples. In the given example the corresponding angular deviation of the beam border was found to be less than 1 mrad near the anode (2 MV equipotential surface). Between the grid and the anode $\psi_1 \geq 0$ was used in the beam equations, where $\psi_1 = 0$ at the grid. This corresponds to a radially increasing potential ($\vartheta \geq 0$) in the beam, which in effect slightly overcompensates the magnetic force and reduces the beam convergence caused by $\vartheta = 0$ near the cathode. The proper shape of the anode surface was achieved by a suitable choice of the initial condition for ψ_1' at the grid and the separation parameter λ_1, which are not otherwise determined. In the same way Fig.5 was obtained, which corresponds to a smaller beam radius.

The author wishes to thank Dr. W. Ott for many useful discussions and experimental information. He is indebted to Dr. P.Merkel and Dr. C.Andelfinger for critical reading of this report. He would also like to thank Dr. H.Tasso and Dr. K.U.v.Hagenow for stimulating suggestions, E.Springmann for computational assistance and various other colleagues.

6. References

1 K. Amboss, The analysis of dense electron beams, Adv.in Electr. and Electr.Phys., Vol.26, 1969, p.1.

2 C. Andelfinger, E. Buchelt, W. Ott and G. Siller, Comparison between laser electron source and febetron, Contr.to the 3rd Work Meeting on ERA, KFK, Ext.Rep.3/69-30, 1969.

3 C. Andelfinger, W. Dommaschk, W. Ott, M. Ulrich, Attempts to improve the field emission source, Proc.of the 4th Work Meeting on ERA, IPP 0/3, 1971, p.34.

4 C. Andelfinger, E. Buchelt, W. Dommaschk, W. Ott, G. Siller, P. Ulbricht, Development of high current electron sources for an electron ring accelerator, 8th Int.Conf. on High Energy Accel., CERN,Geneva 1971.

5 C. Andelfinger, W. Dommaschk, W. Ott, Bright high current 2 MeV electron beam tube working in a poor vacuum, 5th Int.Symp. on Discharges and el. Insulation in Vacuum, Poznan, 1972

6 C. Andelfinger, W. Ott, Entwicklung einer 1 kA, 2 MeV Elektronenröhre, IPP 0/13, 1972.

7 J.E. Boers, Digital computer analysis of axially symmetric electron guns, IEEE Transact. on Electr. Dev., 1965, p.425.

8 P.R. Garabedian, Stability of Cauchy's problem in space for analytic systems of arbitrary type, Journ.Math.Mech., Vol.9, 1960, p.905.

9 W. Glaser, Handb.d.Phys., Vol.33, Berlin 1956, p.382.

10 K.J. Harker, Determination of electrode shapes for axially symmetric electron guns, J.Appl.Phys., Vol.31, 1960, p.2165.

11 E. Madelung, Die mathematischen Hilfsmittel des Physikers, Berlin 1964, p.232.

12 W.H. McNeill, J.R. Uglum, Dynamics of electron beams flow from pulsed, high current field emission cathodes, IEEE Trans.Nucl.Sci., Vol.S-16, 1969, p.70.

7. Appendix

Figure captions:

Fig. 1a,b Illustration of the potential continuation method in the real z-ζ plane and in the corresponding fictitious x-y-v space.

Fig. 2 Mesh pattern for eq.(48)

Fig. 2a Comparison between two different methods of potential continuation from an electron beam to the space charge free region outside. Beam current 500 A, initial beam radius 2.5 cm.

Fig. 3 Potential continuation from a 1000 A beam. Initial beam radius 2.5 cm, virtual beam focus distance at second grid +3.4 m (focusing).

Fig. 4 Beam current 1000 A, initial beam radius 1.5 cm. 2 MV equipotential surface to be used as anode without a grid. Virtual beam focus distance in the corresponding anode aperture approx. -50 cm (defocusing).

Fig. 5 Beam current 1000 A, initial beam radius 1 cm, 2.12 MV equipotential surface to be used as anode without grid. Virtual beam focus distance in the aperture approx. -40 cm (defocusing).

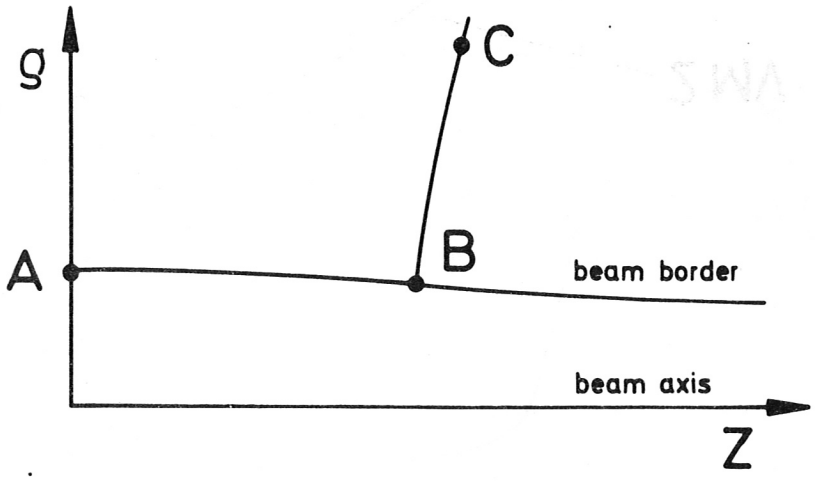

Fig. 1a

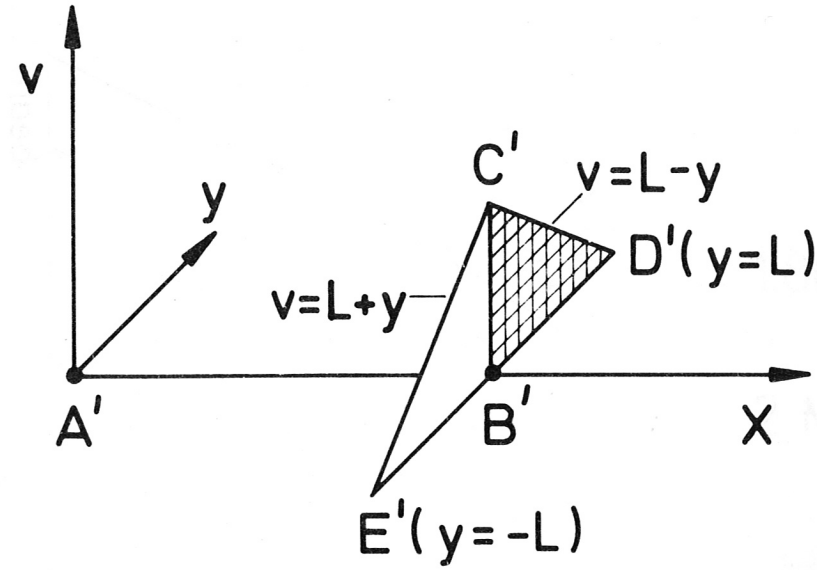

Fig. 1b

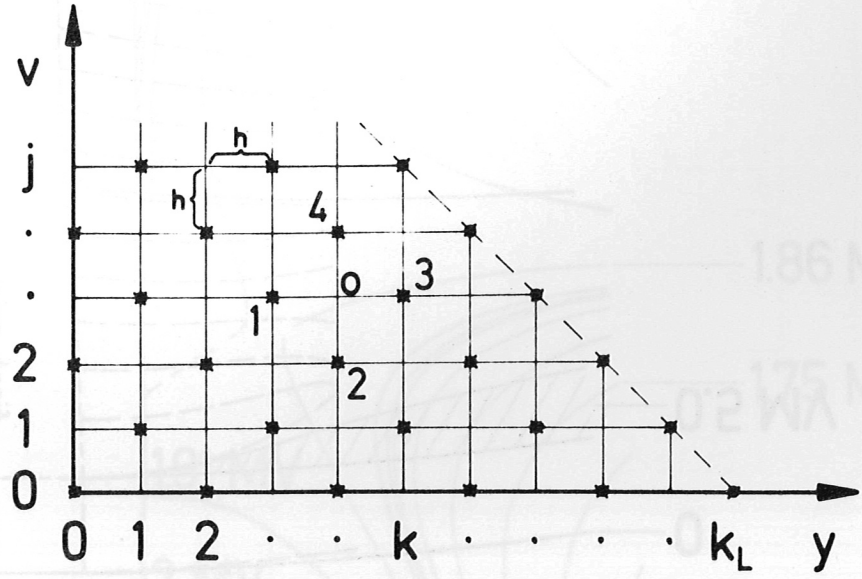

Fig. 2

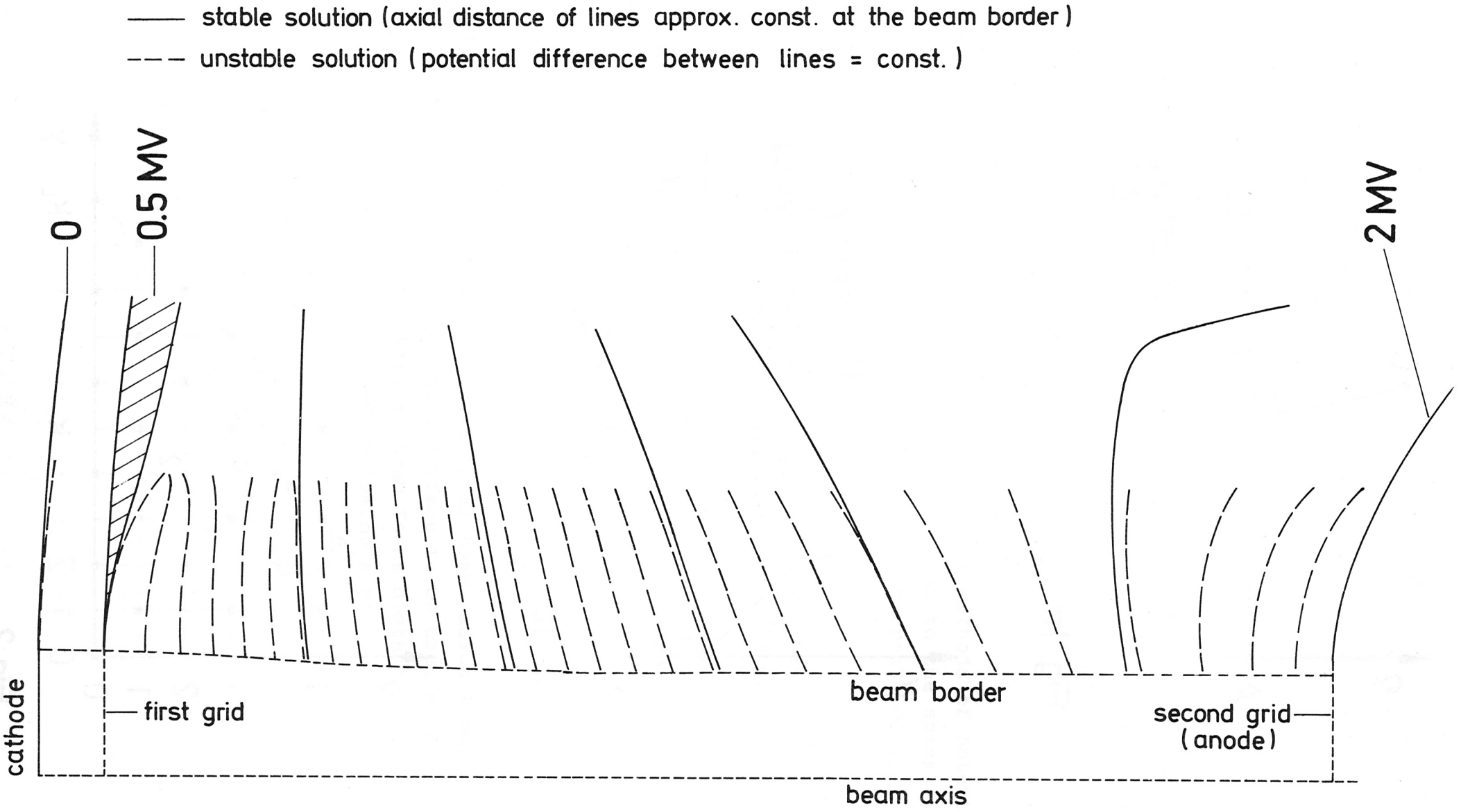
stable solution (axial distance of lines approx. const. at the beam border)
unstable solution (potential difference between lines = const.)
0
0.5 MV
2 MV
cathode
first grid
beam border
second grid
(anode)
beam axis

Fig. 2 a

Fig. 3

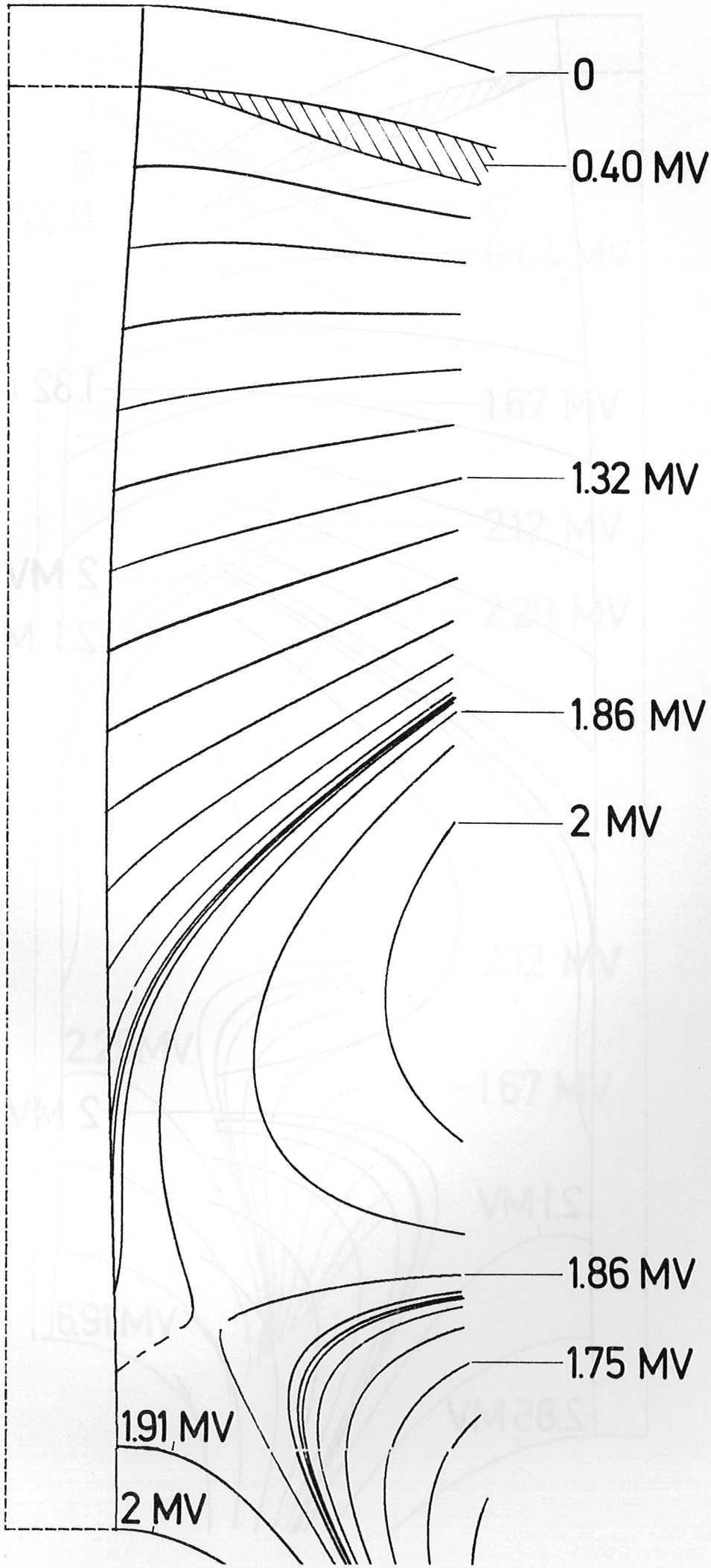

Fig. 4

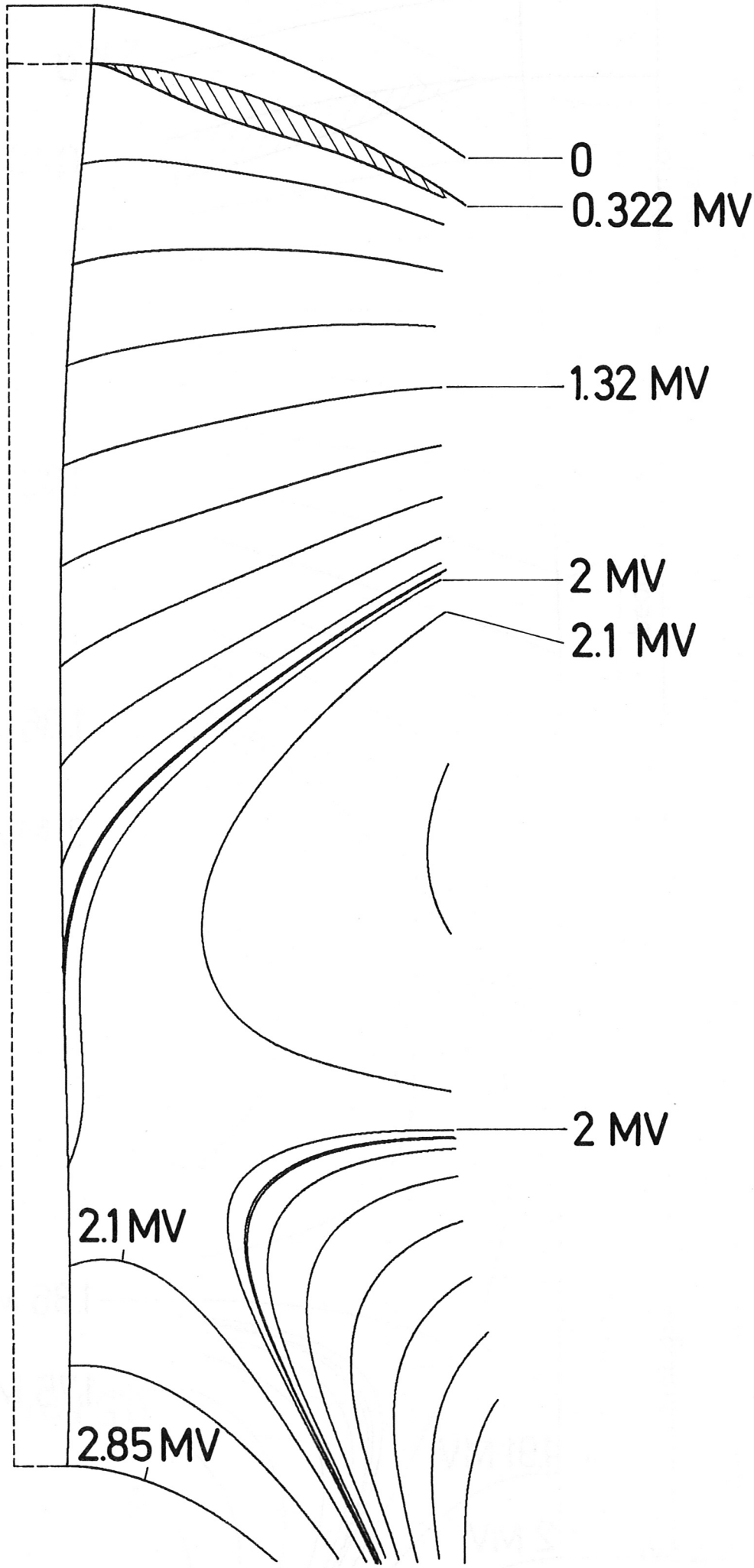

Fig. 5